Supplementary materials

Pd Single Atoms on Nitrogen-Doped Porous Carbon Nanofibers for Efficient Photothermal Catalytic Hydrogenation of Phenylacetylene

Tingting Yang[a], Huaike Li[a], Xuefeng Zhang[b], Guichu Yue[c], Ying Zhang[a], Long Ju[a], Ziyue Zhang[a], Nü Wang[a], Zhimin Cui[a,] and Yong Zhao[a,]**

[a]State Key Laboratory of Bioinspired Interfacial Materials Science, Laboratory of Bio-inspired Smart Interfacial Science and Technology of Ministry of Education, Beijing Advanced Innovation Center for Biomedical Engineering, School of Chemistry, Beihang University, Beijing 100191, PR China

[b]School of Materials Science and Engineering, University of Scienceand Technology of China, Shenyang 110016, P.R. China

[c]College of Chemical Engineering, Inner Mongolia University of Technology, Hohhot 010051, China

E-mail: cuizhm@buaa.edu.cn; zhaoyong@buaa.edu.cn

Chemicals

Zinc nitrate hexahydrate and Lindlar catalyst were obtained from Aladdin Co., Ltd. (Shanghai, China). 2-Methylimidazole (MeIM), commercial Pd/C, phenylacetylene (PA), styrene (ST), ethylbenzene (EB), 3-methylphenylacetylene, 4-methoxystyrene, 4-vinylbiphenyl, 1,3,5-trimethylbenzene (mesitylene), ammonia borane (AB), 4-pentylphenylacetylene, 4-phenyl-1-butyne, 3-chlorophenylacetylene, 4-bromophenylacetylene, 3-ethynylthiophene, 2-ethynylnaphthalene, and 4-ethynylbiphenyl were purchased from Macklin Biotech Co., Ltd. (Shanghai, China). N, N-dimethylformamide (DMF), anhydrous methanol, ethanol, and isopropanol (IPA) were acquired from Beijing Chemical Works (Beijing, China). Polyacrylonitrile (PAN, Mw = 150000) was procured from Sigma-Aldrich Co., Ltd. (USA). Palladium (II) bis(hexafluoroacetylacetonate) [$Pd(C_5HF_6O_2)_2$] and formaldehyde solution were sourced from Strem Chemicals, Inc. (USA). All reagents were analytical grade and used without further purification.

Supporting Figures

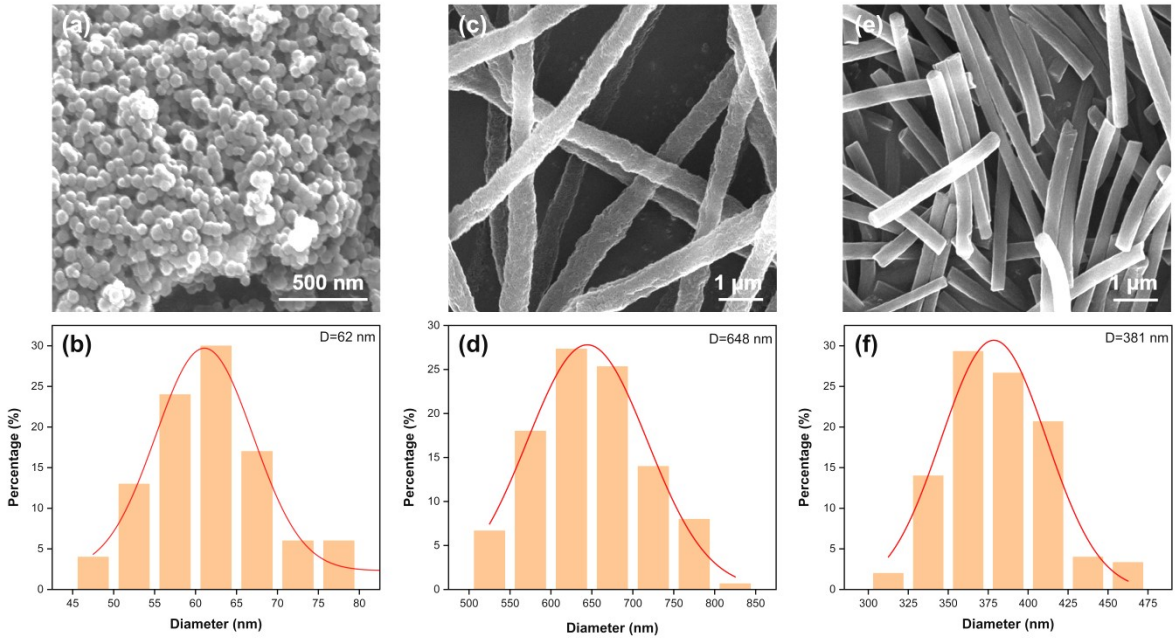

Figure S1. (a, b) The SEM image and particle size distribution of ZIF-8; (c, d) The SEM image and diameter distribution of Pd_1/PCNF; (e, f) The SEM image and diameter distribution of Pd_1/CNF. The average particle size of ZIF-8 is about 62 nm. For the electrospun nanofibrous catalysts, the average diameter of Pd_1/PCNF is approximately 648 nm, while that of Pd_1/CNF is around 381 nm. The larger fiber diameter of Pd_1/PCNF is attributed to the introduction of ZIF-8 nanoparticles, which alters the rheological properties of the precursor solution, leading to thicker fibers during electrospinning.

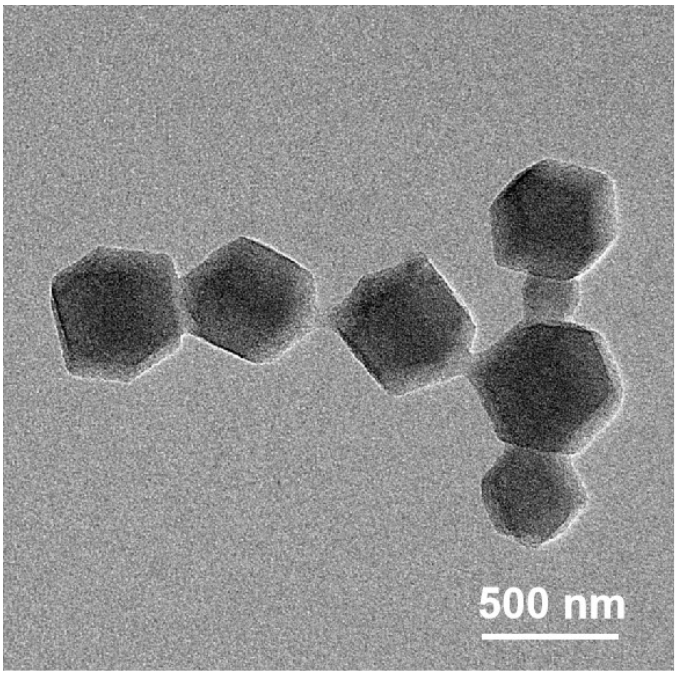

Figure S2. The TEM image of ZIF-8. ZIF-8 exhibits polyhedral nanoparticle morphology with well-defined edges and uniform geometric shapes.

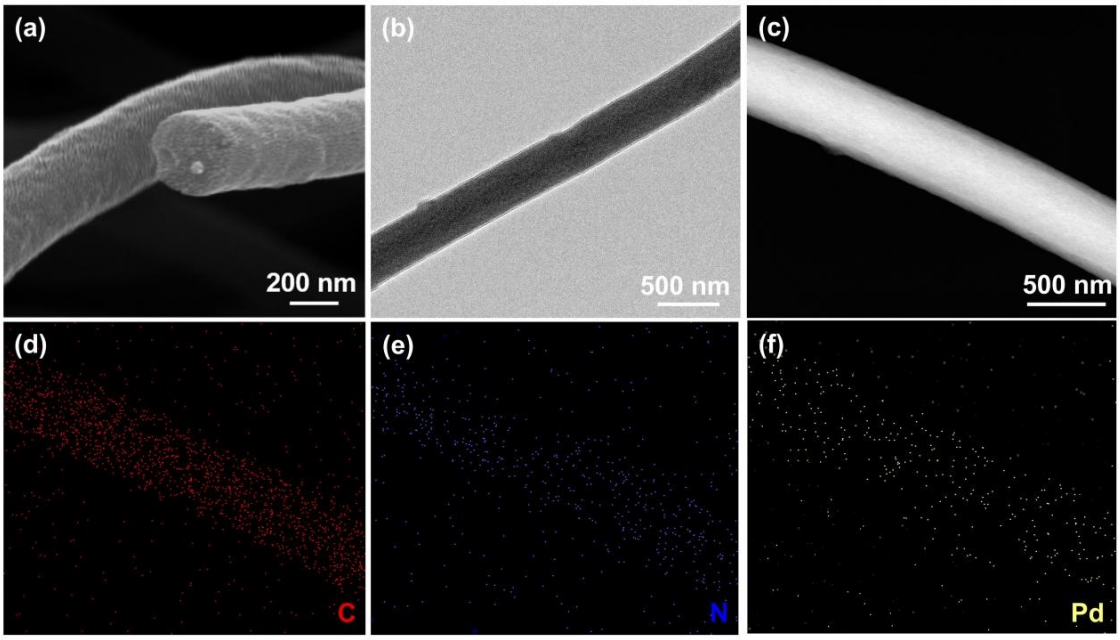

Figure S3. (a) The SEM image of Pd_1/CNF; (b) The TEM image of Pd_1/CNF; (c) The HAADF-STEM image of Pd_1/CNF; (d-f) Element mapping images of C, N, Pd in Pd_1/CNF. Pd_1/CNF exhibits a well-defined fibrous morphology with a smooth surface, and the C, N, and Pd elements are uniformly distributed throughout the fibers.

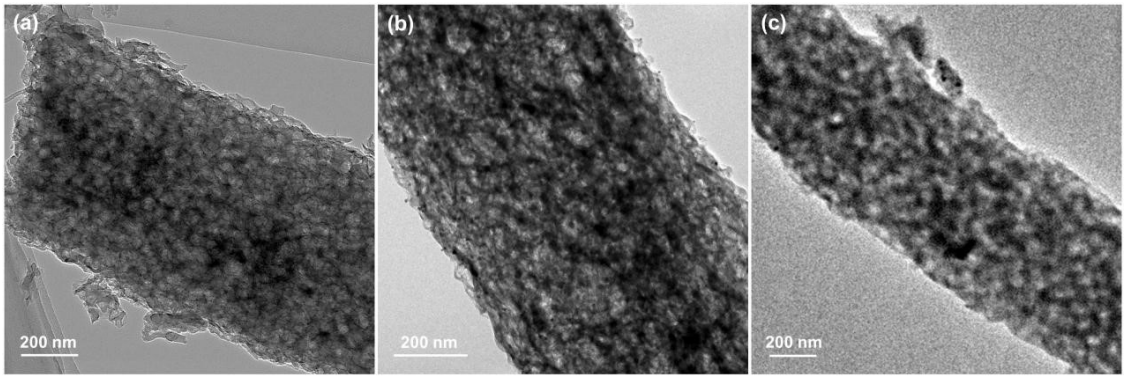

Figure S4. The TEM images of (a) Pd/PCNF-6, (b) Pd/PCNF-14 and (c) Pd/PCNF-30. As the number of ALD cycles increases, the particle size of Pd demonstrates a gradual increasing trend.

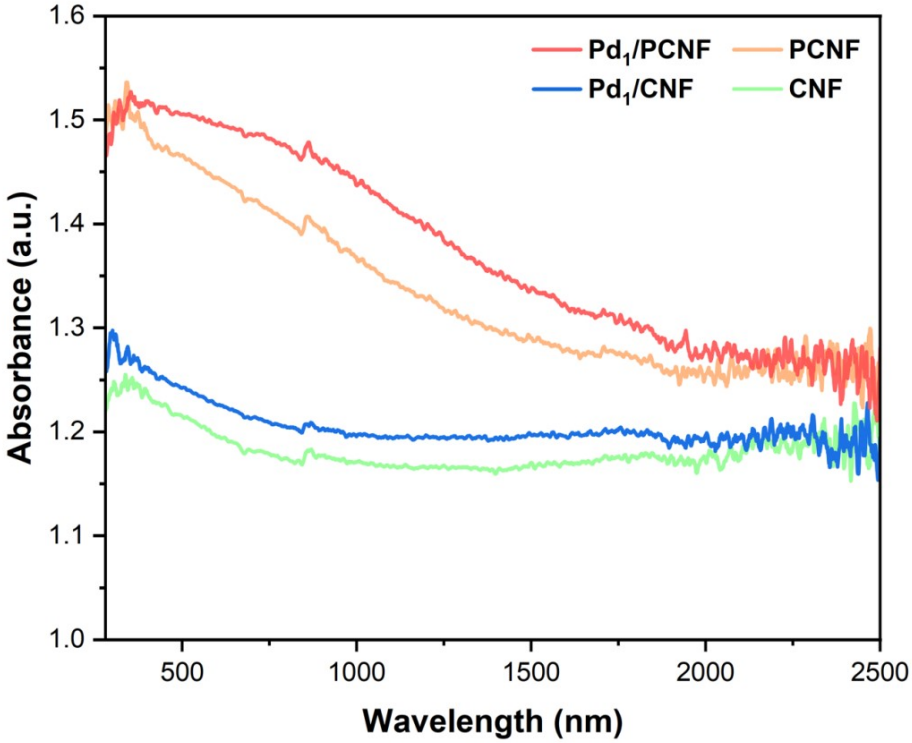

Figure S5. UV-vis-NIR absorption spectra of Pd_1/PCNF, Pd_1/CNF, PCNF and CNF. All four materials exhibit light absorption properties across the entire solar spectral range. Among them, the PCNF system, due to its high specific surface area and porous structure, shows a significantly superior light-harvesting ability compared to the CNF system.

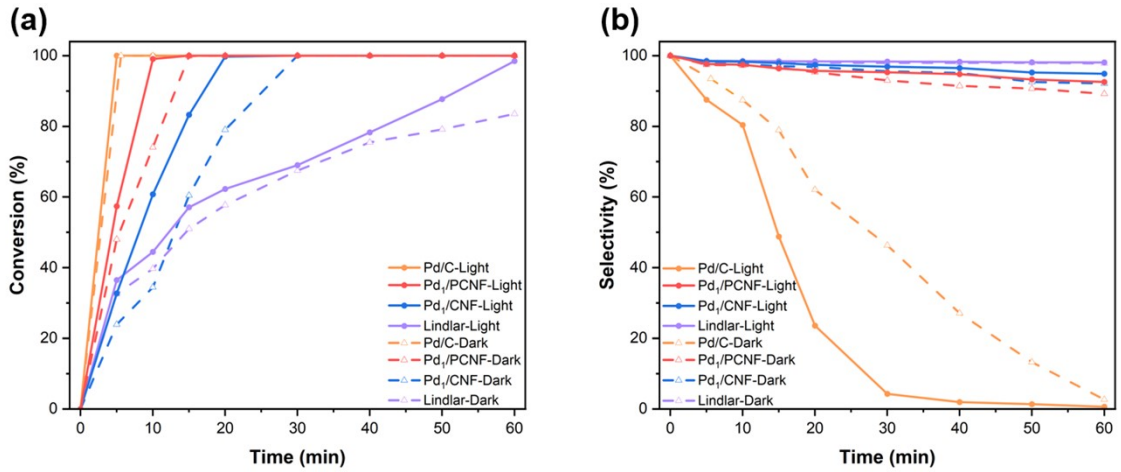

Figure S6. (a) Phenylacetylene conversion and (b) styrene selectivity on various Pd catalysts under different conditions. In the photothermal catalytic selective hydrogenation system of phenylacetylene, the catalytic activities of the four catalysts under light irradiation are all higher than those under dark environment, indicating that light assistance exerts an enhancing effect on the hydrogenation reaction activity. Among them, the Pd_1/PCNF catalyst exhibits the most excellent comprehensive performance: under light irradiation, this catalyst can not only achieve the complete conversion of phenylacetylene within a relatively short time, but also maintain a relatively high styrene selectivity throughout the process, effectively suppressing the side reaction of over-hydrogenation to form ethylbenzene. Its comprehensive catalytic performance is significantly superior to those of the Pd/C, Lindlar catalysts, and the Pd_1/CNF catalyst. Specifically, although the Pd/C catalyst shows relatively high initial activity under light irradiation, its styrene selectivity decreases significantly with the extension of reaction time, and the over-hydrogenation problem is rather prominent; in contrast, the Lindlar catalyst and the Pd_1/CNF catalyst display relatively low catalytic activities, and it is difficult to achieve the desired conversion rate within the same reaction time.

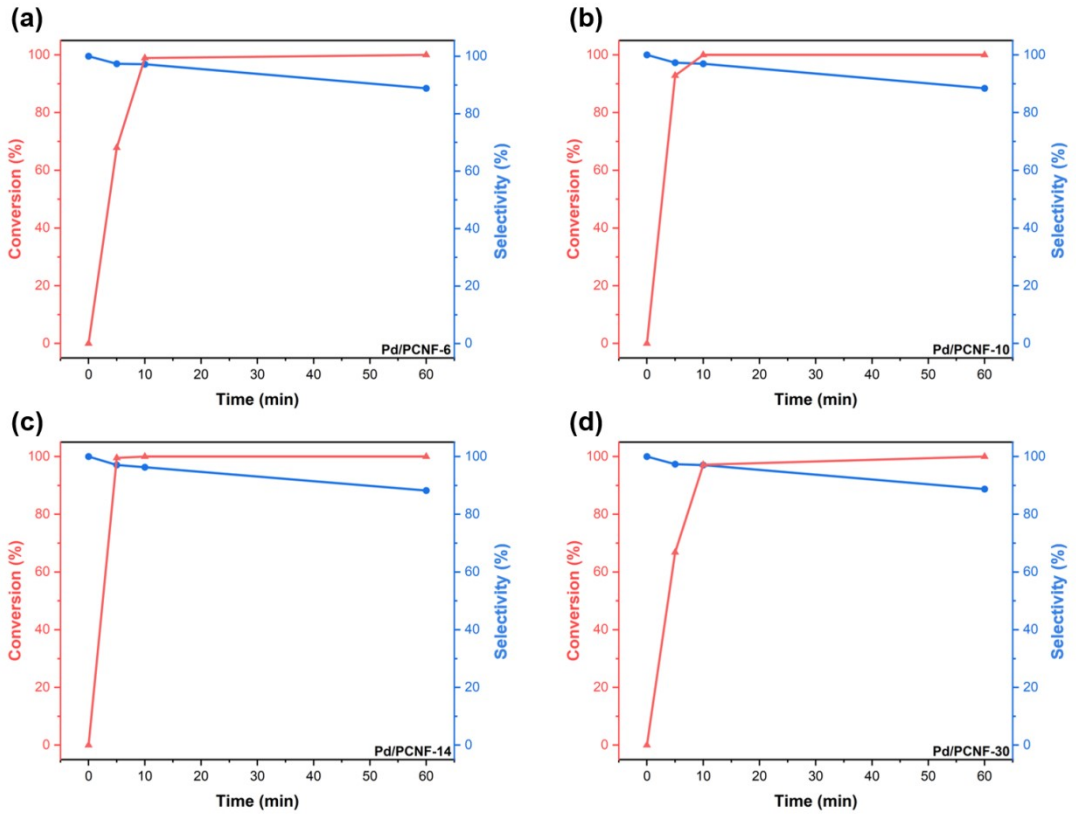

Figure S7. Conversion and selectivity of phenylacetylene hydrogenation on (a) Pd/PCNF-6, (b) Pd/PCNF-10, (c) Pd/PCNF-14, (d) Pd/PCNF-30. For the series of Pd/PCNF-N (N = 6, 10, 14, 30) catalysts in the selective hydrogenation reaction of phenylacetylene, the catalytic activity first increases rapidly and then its growth rate slows down as the number of ALD cycles increases. When the number of ALD cycles is excessively high, the catalytic activity decreases.

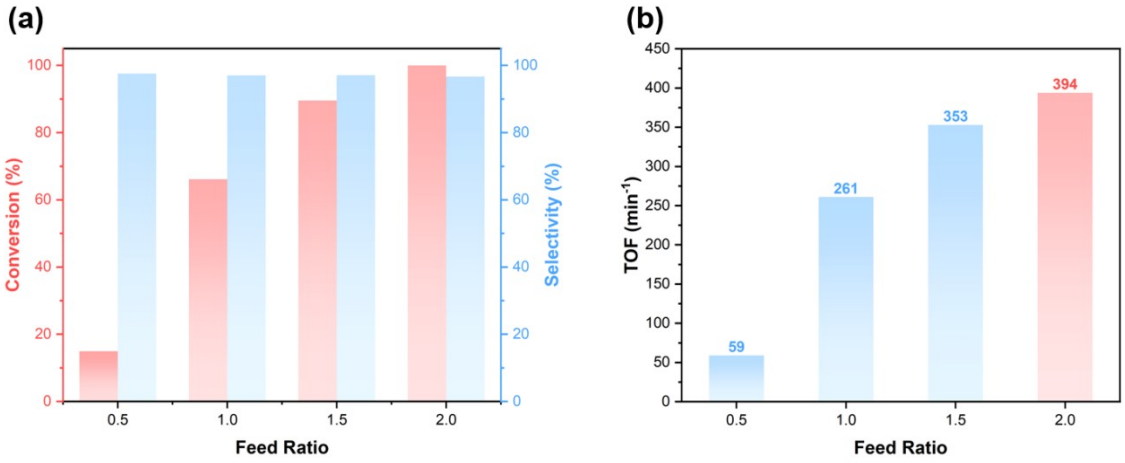

Figure S8. (a) Conversion, selectivity and (b) TOF of phenylacetylene hydrogenation under different AB/PA molar ratios. In the selective hydrogenation of phenylacetylene, the molar ratio of the reducing agent (AB) to the substrate (PA) exerts a regulatory effect on the catalytic performance. With the increase in the AB/PA molar ratio, both the reaction conversion and TOF show a positively correlated growth trend, indicating that the sufficiency of the reducing agent is a key factor influencing the reaction efficiency. The 2:1 ratio, which is widely adopted in the literature, has been verified as the optimal balance point between activity and practicality. Thus, this ratio was selected as the reaction condition in this study.

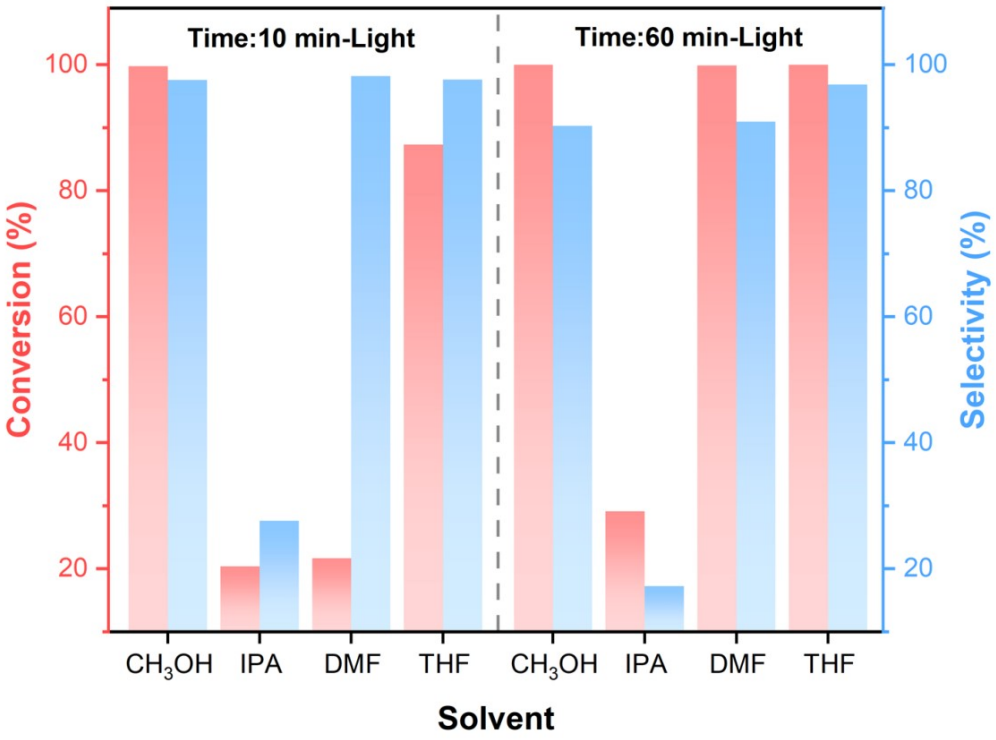

Figure S9. Conversion and selectivity of phenylacetylene hydrogenation over Pd_1/PCNF in different solvents. In the photothermal catalytic selective hydrogenation of phenylacetylene, the performance of the Pd_1/PCNF catalyst exhibits remarkable solvent dependence. When methanol (CH_3OH) or tetrahydrofuran (THF) is used as the solvent, the catalyst can achieve high conversion and excellent selectivity. Conversely, when isopropanol (IPA) or N, N-dimethylformamide (DMF) is used as the solvent, the catalytic performance is significantly reduced.

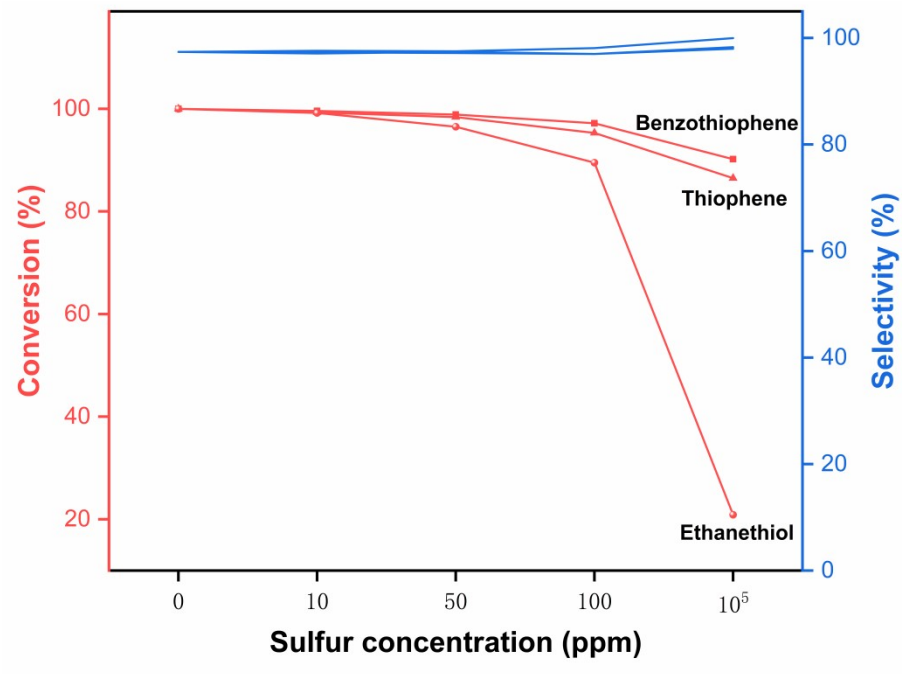

Figure S10. Catalytic performance of Pd_1/PCNF for the selective hydrogenation of phenylacetylene in the presence of different sulfur impurities. **10 ppm:** Represents a low sulfur content commonly found in deeply desulfurized industrial feedstocks. **50 ppm:** Represents a typical sulfur content after conventional hydrodesulfurization. **100 ppm:** Represents a high-sulfur scenario or insufficiently purified streams. **10^5 ppm:** This concentration far exceeds typical industrial levels and is employed as an extreme test condition to probe the intrinsic tolerance limit of the catalyst and the nature of its poisoning mechanisms.

The Pd_1/PCNF catalyst exhibits excellent tolerance toward reversibly poisoning sulfur impurities such as thiophene and benzothiophene. At a sulfur concentration of 100 ppm, the catalyst retains over 95% of its initial activity, with slightly better tolerance observed for benzothiophene than for thiophene. This is likely attributed to the hierarchical porous structure of the carbon nanofiber support, which hinders the diffusion of bulkier benzothiophene molecules and partially shields the Pd single-atom sites from deactivation. In contrast, the catalyst is more sensitive to ethanethiol, a strongly coordinating small-molecule sulfur compound. At 100 ppm, the conversion decreases to 89.5%, and further increases to 10^5 ppm result in a sharp drop to 20.9%, confirming an irreversible poisoning mechanism via the formation of strong Pd-S bonds. Overall, although the catalytic performance of Pd_1/PCNF experienced a slight decrease with increasing concentrations of sulfur-containing impurities, it still demonstrates promising potential for practical applications within industrial feedstocks.

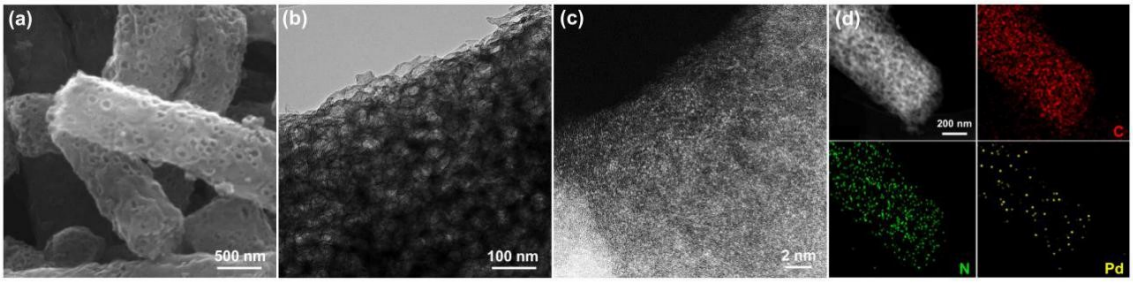

Figure S11. The (a) SEM image, (b) TEM image, (c) AC-HAADF-STEM image and (d) element mapping images of C, N, Pd in Pd_1/PCNF after the selective hydrogenation of phenylacetylene. After 5 reaction cycles, the pore structure of the catalyst remains intact, and no aggregation of single atoms occurs, demonstrating good structural stability.

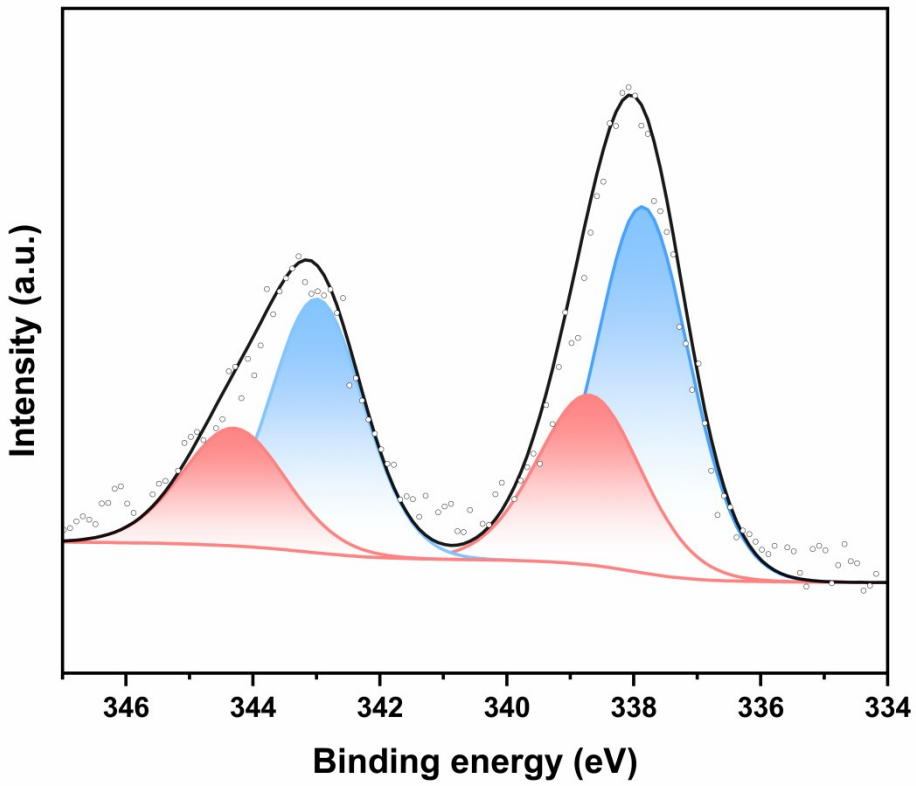

Figure S12. Pd 3d XPS spectra of Pd_1/PCNF after 5 reaction cycles. The Pd species retained their electron-deficient state ($Pd^{\delta+}$) and no characteristic peaks corresponding to metallic Pd^0 are detected.

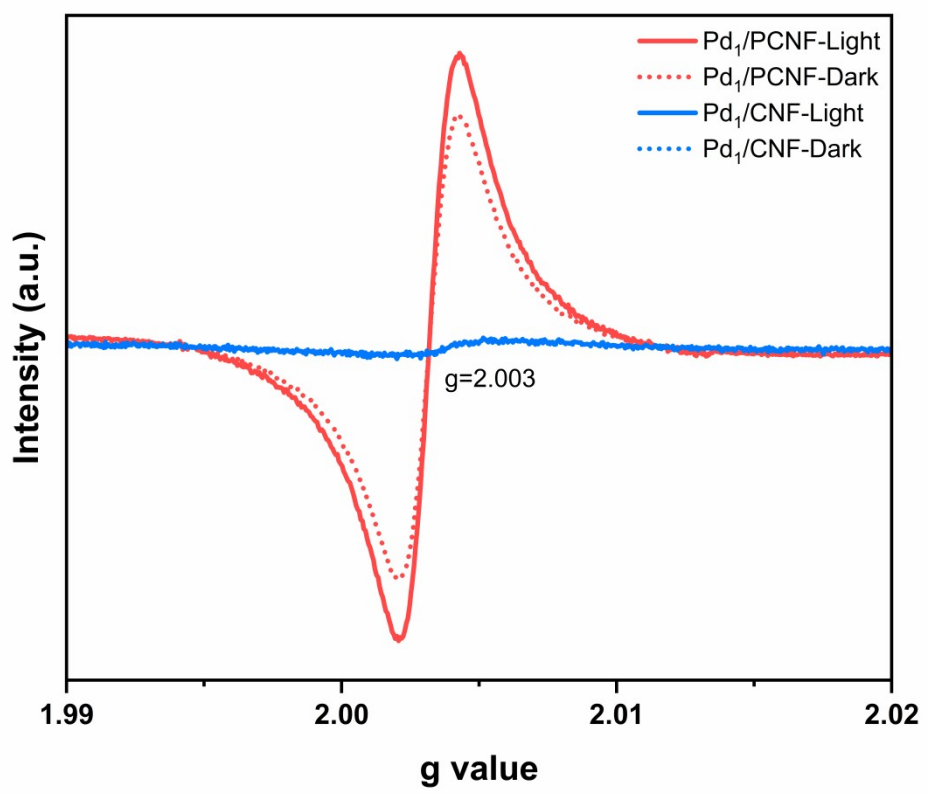

Figure S13. The EPR spectra of Pd_1/PCNF and Pd_1/CNF. Under dark conditions, the Pd_1/PCNF catalyst exhibits a distinct EPR signal at $g \approx 2.003$, which can be attributed to localized unpaired electrons associated with carbon defects or nitrogen-doped sites within the porous carbon framework. Upon simulated solar irradiation, the intensity of this EPR signal increases, indicating effective separation of photogenerated electrons and holes. In contrast, the non-porous Pd_1/CNF catalyst displays a significantly weaker EPR signal under identical conditions, and the photoinduced enhancement is considerably less pronounced.

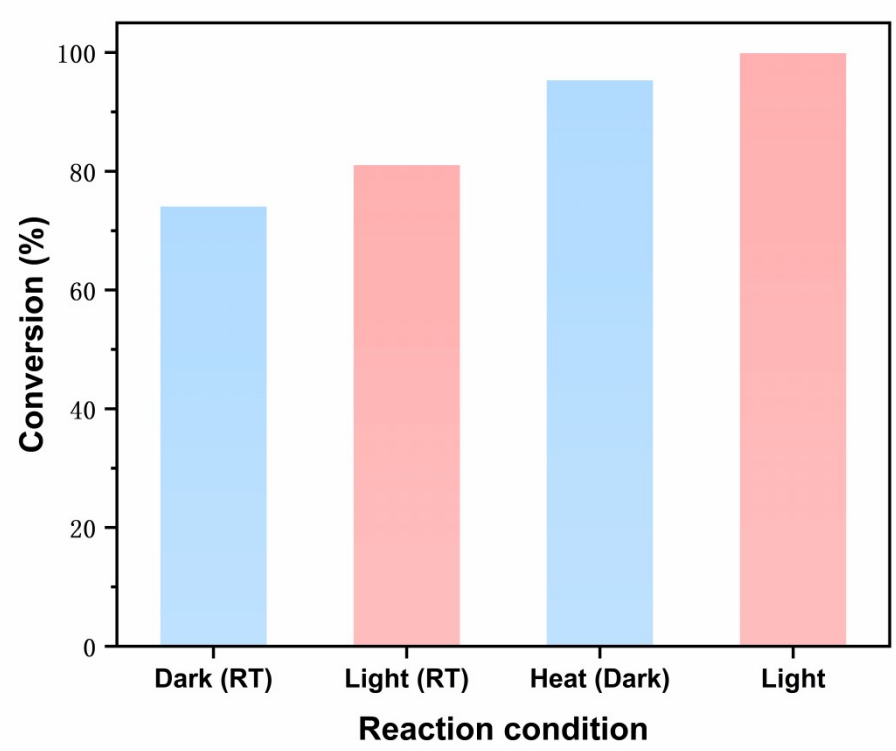

Figure S14. Conversion of phenylacetylene selective hydrogenation over Pd_1/PCNF under different reaction conditions. Performance enhancement under light is due to synergistic photonic-thermal contributions, where thermal dominates and photonic assists.

Supporting Tables

Table S1. Pd loading amounts on different catalysts determined by ICP-MS.

Samples	Pd_1/CNF	Pd_1/PCNF	Pd/PCNF-6	Pd/PCNF-10	Pd/PCNF-14	Pd/PCNF-30
Pd loadings (wt%)	0.11	0.18	0.27	0.48	0.70	1.58

Table S2. Catalytic Performance Comparison: Pd_1/PCNF vs. Reported Metal Catalysts in Phenylacetylene Semi-Hydrogenation.

Entry	Catalyst	Catalytic type	Hydrogen source	Con./%	Sel./%	TOF/min^{-1}	Ref.
1	Pd_1/PCNF	Photothermal	NH_3BH_3	>99	97.4	586	This work
2	CuPd@ZIF-8	Photothermal	NH_3BH_3	99	96	6799	[1]
3	Pd/DCN	Photo	NH_3BH_3	100	>99	2002	[2]
4	Au/BT	Photo	H_2	>99	99	16.9	[3]
5	Pd/TiO_2-ICT	Photo	CH_3OH	99	98	14.2	[4]
6	Pd-$SrTiO_3$	Photo	CH_3OH	100	>99	N.R.	[5]
7	L-lysine/Ni/Nb_2O_5	Photo	H_2	>99	95.8	N.R.	[6]
8	Pd/mNCNFs	Thermal	NH_3BH_3	100	96	10.2	[7]
9	Pd@UiO-66 (Hf)	Thermal	NH_3BH_3	100	93.2	2.4	[8]
10	$NiZn_3$/AlSBA-15	Thermal	H_2	99.6	90.3	653.4	[9]
11	Pd_1@ZSM-5	Thermal	H_2	100	96	559.7	[10]
12	Pd@PPy-600	Thermal	H_2	99	96	81.9	[11]
13	$Pt_{0.2}$@ZSM-22	Thermal	H_2	>99	91	97.7	[12]
14	Pd/NTs	Thermal	H_2	100	97.4	57.6	[13]
15	Ni/Pd	Thermal	H_2	100	97.3	59.4	[14]

16	Co clusters/N-C	Thermal	H_2	99	92	52.2	[15]
17	Pd-Pb NSs	Thermal	H_2	100	95.8	37.6	[16]
18	H_{350}-Ni/COF	Thermal	H_2	>99	85	28.2	[17]
19	Pd_1/BP	Thermal	H_2	100	99	18	[18]
20	$Pt/PSiO_2$	Thermal	H_2	72	87.5	6.6	[19]
21	Au/GO	Thermal	H_2	99	99	6	[20]

References

[1] L. Li, W. Yang, Q. Yang, Q. Guan, J. Lu, S. Yu, H. Jiang, ACS Catal. 10 (2020) 7753-7762.

[2] Y. Hu, S. Zhang, Z. Zhang, H. Zhou, B. Li, Z. Sun, X. Hu, W. Yang, X. Li, Y. Wang, S. Liu, D. Wang, J. Lin, W. Chen, S. Wang, Adv. Mater. 35 (2023) 2304130.

[3] Q. Bi, E. Song, J. Chen, M. Riaz, M. Zhu, J. Liu, Y. Han, F. Huang, Appl. Catal. B: Environ. 309 (2022) 121222.

[4] W. Jia, H. Wang, C. Xue, Y. Li, Q. Xiao, ACS Appl. Nano Mater. 8 (2025) 11095-11103.

[5] B. Yang, K. Liu, Y. Ma, J. Ma, Y. Chen, M. Huang, C. Yang, Y. Hou, S. Hung, J. Yu, J. Zhang, X. Wang, Angew. Chem. Int. Ed. 63 (2024) e202410394.

[6] J. Wang, M. Wang, X. Li, X. Gu, P. Kong, R. Wang, X. Ke, G. Yu, Z. Zheng, Appl. Catal. B: Environ. 313 (2022) 121449.

[7] H. Li, S. Li, G. Yue, S. Gao, X. Zhang, K. Zhu, T. Yang, Z. Zhang, N. Wang, J. Bai, Z. Cui, Y. Zhao, J. Mater. Chem. A 12 (2024) 31612-31618.

[8] V. Bakuru, B. Velaga, N. Peela, S. Kalidindi, Chem. Eur. J. 24 (2018) 15978-15982.

[9] L. Yang, S. Yu, C. Peng, X. Fang, Z. Cheng, Z. Zhou, J. Catal. 370 (2019) 310-320.

[10] H. Liu, J. Li, X. Liang, H. Ren, H. Yin, L. Wang, D. Yang, D. Wang, Y. Li, J. Am. Chem. Soc. 146 (2024) 24033-24041.

[11] R. Zhang, Z. Liu, S. Zheng, L. Wang, L. Zhang, Z. Qiao, Adv. Mater. 35 (2023) 2209635.

[12] J. Tang, P. Liu, X. Liu, L. Chen, H. Wen, Y. Zhou, J. Wang, ACS Appl. Mater. Interfaces 12 (2020) 11522-11532.

[13] S. Domínguez-Domínguez, Á. Berenguer-Murcia, B. Pradhan, Á. Linares-Solano, D. Cazorla-Amorós, J. Phys. Chem. C 112 (2008) 3827-3834.

[14] S. Domínguez-Domínguez, Á. Berenguer-Murcia, D. Cazorla-Amorós, Á. Linares-Solano, J. Catal. 243 (2006) 74-81.

[15] Q. Zhu, X. Lu, S. Ji, H. Li, J. Wang, Z. Li, 405 (2022) 499-507.

[16] C. Shen, Y. Ji, P. Wang, S. Bai, M. Wang, Y. Li, X. Huang, Q. Shao, ACS Catal. 11 (2021) 5231-5239.

[17] N. Wang, J. Liu, M. Zhang, C. Wang, X. Li, L. Ma, ACS Appl. Mater. Interfaces 13 (2021) 60135-60143.

[18] C. Chen, W. Ou, K. Yam, S. Xi, X. Zhao, S. Chen, J. Li, P. Lyu, L. Ma, Y. Du, W. Yu, H. Fang, C. Yao, X. Hai, H. Xu, M. Koh, S. Pennycook, J. Lu, M. Lin, C. Su, C. Zhang, J. Lu, Adv. Mater. 33 (2021) 2008471.

[19] S. Jayakumar, A. Modak, M. Guo, H. Li, X. Hu, Q. Yang, Chem. Eur. J. 23 (2017) 7791-7797.

[20] L. Shao, X. Huang, D. Teschner, W. Zhang, ACS Catal. 4 (2014) 2369-2373.